Acta metall. Vol. 33, No. 3, pp. 409–422, 1985
Printed in Great Britain

0001-6160/85 $3.00 + 0.00
Pergamon Press Ltd

CONSTRAINED CREEP CAVITATION OF GRAIN BOUNDARY FACETS

P. M. ANDERSON and J. R. RICE
Division of Applied Sciences, Harvard University, Cambridge, MA 02138, U.S.A

(*Received* 18 *September* 1984)

Abstract—Constraints on diffusive creep cavity growth along grain boundary facets are studied for the limiting case when all facets oriented approximately normal to an applied tensile load are uniformly cavitated. This situation represents the opposite limiting case to when cavitated facets are well-separated and do not interact with each other. The analysis is done for a 3-D periodic polycrystalline model of grains in the shape of the Wigner–Seitz cells of a f.c.c. lattice. The grains have freely-sliding boundaries and deform in a nonlinear viscous manner in response to applied stress. Expressions for the cavity growth rate and the strain and time to rupture are compared with results of prior work in which cavitated facets are well-separated, and this gives a good understanding of the ranges of stress and temperature over which cavity growth is constrained and rupture lifetime is increased. The time to rupture, which is taken here to mean cavity coalescence on the damaged facets, is seen to depend strongly on the proximity of cavitated facets, at least when cavity growth is constrained. However, the strain to rupture is observed to lack this strong dependence although for constrained conditions, the cavitation process contributes substantially to the total strain when cavitated facets are closely-spaced. When cavitated facets are well-separated, the polycrystal is seen to achieve a relatively constant strain rate. By comparison, the strain rate is seen to vary substantially with time when cavitated facets are closely-spaced. The time and strain to rupture as well as strain rate versus time curves are calculated as functions of applied load and temperature for nickel as a representative f.c.c. metal.

Résumé—Nous étudions l'effet de contraintes sur la croissance des cavités de fluage de diffusion le long de facettes intergranulaires dans le cas limite où toutes les facettes orientées approximativement perpendiculairement à une contrainte de traction appliquée présentent une cavitation uniforme. Cette situation est l'opposée du cas limite où les facettes présentant la cavitation sont bien séparées et n'interagissent pas entr'elles. Nous avons effectué l'analyse pour un modèle polycristallin périodique à trois dimensions de grains ayant la forme des cellules de Wigner et Seitz d'une structure c.f.c. Les grains présentent des joints qui glissent librement et ils se déforment de manière visqueuse non linéaire sous l'effet d'une contrainte appliquée. Nous comparons les expressions pour la vitesse de croissance des cavités, la déformation et la durée de vie à la rupture avec les résultats d'un travail antérieur dans lequel les facettes présentant la cavitation sont bien séparées; ceci conduit à une bonne compréhension des domaines de contrainte et de température dans lesquels la croissance des cavités est gênée et où la durée de vie à la rupture est augmentée. On voit que la durée de vie à la rupture, que est prise ici égale au temps moyen de coalescence des cavités sur les facettes en dommagées, dépend fortement de la proximité des facettes cavitées, au moins lorsque la croissance des cavités est gênée. Cependant, la déformation à la rupture ne présente pas cette forte dépendance bien que, lorsqu'elle est gênée, la cavitation contribue notablement à la déformation totale lorsque les facettes cavitées sont proches. Lorsque les facettes endommagées sont bien séparées, le polycristal présente une vitesse de déformation ? constante. Au contraire, la vitesse de déformation varie notablement en fonction du temps lorsque les facettes endommagées sont proches. Nous avons calculé la durée de vie et la déformation à la rupture, ainsi que les courbes de la vitesse de déformation en fonction du temps, en fonction de la contrainte appliquée et de la température dans le nickel considéré comme représentatif des métaux c.f.c.

Zusammenfassung—Die Einschränkungen, denen das Hohlraumwachstum während des Diffusionskriechens entlang von Korngrenzfacetten unterliegt, werden für den Grenzfall untersucht, daß sämtliche Facetten ungefähr senkrecht zu einer äußeren Last liegen und gleichmäßig mit Hohlräumen besetzt sind. Diese Bedingungen stehen im Gegensatz zu dem Grenzfall, bei dem die hohlraumbesetzten Facetten deutlich getrennt sind und nicht miteinander wechselwirken. Die Analyse wird in einem 3-D-periodischen polykristallinen Modell aus Körnern in der Form von Wigner–Seitz-Zellen eines kfz. Gitters durchgeführt. Die Körner weisen frei gleitende Grenzen auf und verformen sich nichtlinear und viskos entsprechend der Spannung. Die Ausdrücke für Wachstumsrate der Hohlräume, Bruchdehnung und Bruchstandzeit werden mit Ergebnissen verglichen, die früher für den Fall deutlich getrennter Facetten erhalten wurden. Hieraus ergibt sich eine gute Einsicht in die Temperatur- und Spannungsbereiche, in denen das Hohlraumwachstum eingeschränkt ist und somit die Bruchstandzeit erhöht. Die Bruchstandzeit, bestimmt hier von dem Zusammenwachsen der Hohlräume, hängt stark vom Abstand der hohlraumbesetzten Facetten ab, wenigstens beim eingeschränkten Wachstum. Die Bruchdehnung jedoch weist diese starke Abhängigkeit nicht auf, wenn auch der Prozeß der Hohlraumbildung im Falle des eingeschränkten Wachstums bei nahe beieinanderliegenden Facetten beträchtlich zur Gesamtdehnung beiträgt. Liegen die hohlraumbestzten Facetten deutlich getrennt, dann verformt sich der Polykristall mit einer relativ konstanten Dehnungsrate. Im Vergleich dazu variiert die Dehnungsrate beträchtlich in der Zeit für den Fall nahe beieinanderliegender Facetten. Bruchstandzeit und -dehnung, ebenso der Zusammenhang von Dehnungsrate mit der Zeit, werden für Nickel als repräsentatives kfz. Metall als Funktion der angelegten Last und der Temperatur berechnet.

INTRODUCTION

At elevated temperatures polycrystalline materials generally fracture by the initiation, diffusive growth and eventual coalescence of grain boundary cavities. The basic model for the diffusive growth process is due to Hull and Rimmer [1], who depict a cavitated grain boundary facet as a uniform array of voids (Fig. 1). Many others have contributed to subsequent improvement of the model and have formulated the void growth rate $\dot{a}$ and the average opening rate of the cavitated grain boundary $\dot{\delta}$ in terms of the current void radius a, void spacing $2b$ and the average stress σ_F across the cavitated facet [2]–[9]; see (19) to follow.

However, in applying such relations for $\dot{a}$ and $\dot{\delta}$, it is incorrect to equate σ_F to the stress βS which acts across the grain boundary of an identical but non-cavitating specimen under the same macroscopic stress S [Fig. 2(a)]. Here, β (which we estimate later to be approximately 1.7) is interpretable as a stress enhancement factor, on facets approximately normal to the tensile direction, due to freely-sliding grain boundaries. Consider the geometry of a cavitated facet in a polycrystalline material shown in Fig. 2(b). The cavitated facet there is surrounded solely by uncavitated material to depict the case of relative isolation of one cavitated facet from another. Dyson [10] observed that the opening rate of the cavitated facet must be accommodated by surrounding material, and this may strongly constrain the void growth process, particularly when the cavitated facets are relatively isolated from one another. That is, conditions may exist where the surrounding material is unable to accommodate the cavity opening rate corresponding to $\sigma_F = \beta S$. The load across the cavitated facet is then shed to the surrounding material, reducing σ_F from βS until the opening rate of the facet is compatible with the creep rate of surrounding material. The result under such constrained conditions is that the cavity growth process is slowed, and the time to void coalescence on a cavitated facet is prolonged.

Rice [11] incorporated Dyson's concept to model in an approximate manner void growth in a material with well-separated cavitated facets [Fig. 2(b)], the opening rate of which is accommodated by the dislocation creep of material surrounding the facet. Also, Cocks and Ashby [12] studied the effect of the proximity of cavitated facets to one another over a wide range, and reached similar conclusions in the well-separated regime. The functional form for the average opening rate of a well-separated cavitating facet was assumed as [11]

$$\dot{\delta} = \alpha[(\beta S - \sigma_F)/\beta S]\dot{E}_{\text{nocav}} d. \tag{1}$$

Here $\dot{E}_{\text{nocav}} = \dot{E}_{\text{nocav}}(S)$ is the creep strain rate for stress S acting on an uncavitated polycrystal (in which case $\sigma_F = \beta S$), and d is the diameter of the cavitating facet. The proportionality factor α in (1) depends on the creep exponent n in the relation $\dot{\varepsilon} \propto \sigma^n$ between creep strain rate and stress. Rice estimated that in the absence of grain boundary sliding, values of α would range from about $\alpha = 0.64$ for $n = 1$ to $\alpha = 0.90$ for $n = 5$. Improved estimates for that case were given by He and Hutchinson [13]. Rice noted, however, that the presence of freely-

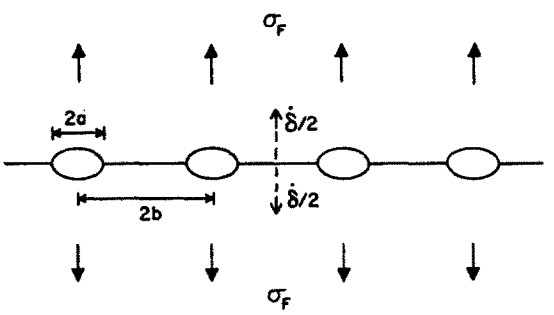

Fig. 1. A cavitated grain boundary, modeled as an array of uniformly spaced voids, subjected to stress σ_F and separating at a rate $\dot{\delta}$ due to diffusional flow of matter from the cavity surfaces to the grain boundary.

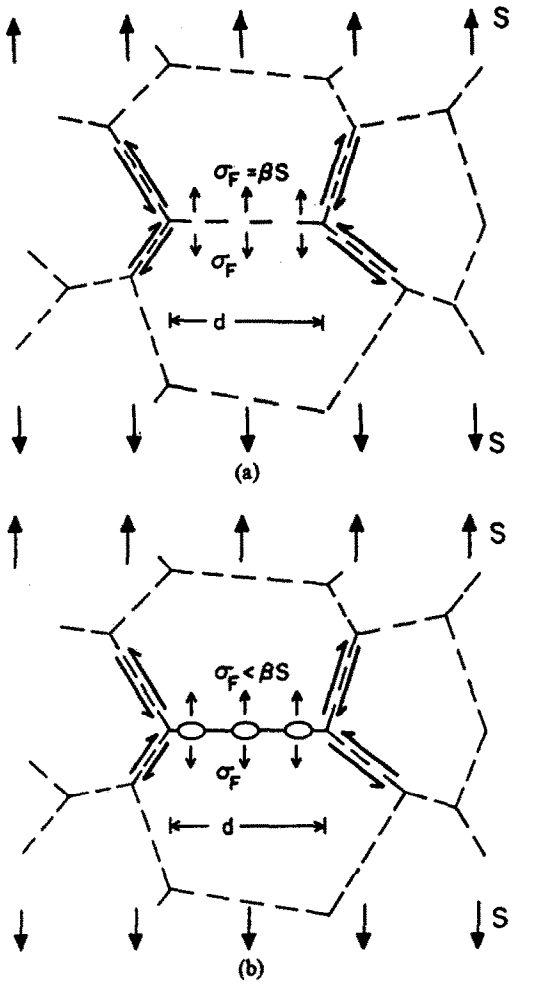

Fig. 2. (a) An uncavitated grain boundary, across which acts a stress $\sigma_F = \beta S$ enhanced by a factor β due to grain boundary sliding. (b) The same grain boundary in (a), but in a cavitated state. Local opening of the grain boundary due to void growth reduces σ_F from the value βS.

sliding grain boundaries would increase α over the previous values, and estimated that perhaps a doubling of the previous α values would then be appropriate. Combining (1) with an equation characterizing the diffusive void growth process for the basic geometry of Fig. 1 [i.e. $\dot{\delta} = \dot{\delta}(\sigma_F)$] enabled solution for σ_F and thus for the cavity growth rate $\dot{a}$ and the time to "rupture" as a function of the applied stress S. Here "rupture" was equated to the coalescence of voids along the cavitated facet.

Rice thus found the degree of constraint to be characterized by a length parameter $L = (\mathscr{D}_b S/\dot{E}_{nocav})^{1/3}$ which decreases with increasing stress and temperature. When L^3 is much greater than b^2d, the compliance of the void growth mechanism exceeds that of the surrounding uncavitated material, the constraint effect discussed herein is important, and rupture lifetime is controlled by the strain rate $\dot{E}_{nocav}$. Here $\mathscr{D}_b = D_b\delta_b\Omega/kT$ is a boundary diffusive parameter for which $D_b\delta_b$ is the grain boundary diffusion coefficient, Ω is the volume per atom, and kT is temperature in energy units. The discussion assumes that $\dot{E}_{nocav}$ has the same temperature dependence as does bulk diffusion, and is proportional to S^n.

Different forms for $\dot{\delta}$ must arise in (1) when the cavitated facets are more closely spaced so that the surrounding material may not be regarded as uncavitated. If $\dot{E}_{nocav}$ is interpreted consistently as the strain rate resulting from stress S applied to an uncavitated polycrystal, the effect will be to substantially increase the factor of proportionality α in (1) due to larger scale interactions between the creep deformability of the grain and grain boundary void growth. This effect can be seen in the equations of Cocks and Ashby [12].

In particular, an opposite limiting case discussed by Dyson [10] occurs when all facets approximately perpendicular to a remotely applied tensile stress are cavitated and again, the grain boundaries slide freely. Such a case represents a lower bound to the constraint effect, and hence an upper bound to the void growth rate in a polycrystalline sample. As such, it constitutes the focus of this study. A functional form for $\dot{\delta}$ similar to (1) is developed for a 3-D polycrystalline model with freely-sliding grain boundaries and with all facets cavitated which are perpendicular to a uniaxial tensile stress. A diffusive cavity growth model is then included in the analysis to obtain criteria as to when constrained cavity growth occurs. Times and strains to rupture are then calculated for pure nickel as a representative f.c.c. metal, and comparison is made between the two opposite limiting cases discussed above so as to provide bounds to actual situations.

CONCEPT OF 3-D CONSTRAINED CAVITY GROWTH

Constraint manifests itself somewhat differently in 3-D than in 2-D. Consider the 2-D hexagonal geometry in Fig. 3 for which grain boundaries are considered freely-sliding. Effectively, the concept of constraint by surrounding material does not exist when all facets perpendicular to an applied stress are cavitated. No deformation of the grains is then required to accommodate the opening rate of the cavitating facets. Hence, constraint in the 2-D case has meaning only for isolated or nonuniform distributions of cavitating facets, or when a regular hexagonal array of grains is not used [14].

A 3-D geometry shows similarities to the 2-D one, except that when deformed, it has additional sliding components located out of the plane of the 2-D representation in Fig. 3. When a structure of 3-D space-filling grains cavitates, grain boundary sliding components that are consistent with the grain symmetry and accommodate the cavitation do not produce compatible displacements without grain deformation. Therefore, a 3-D geometry, unlike a regular 2-D one, permits constraint of the void growth process for the posed limiting case of closely-spaced cavitating facets.

The manner by which surrounding material accommodates the opening rate $\dot{\delta}$ of the cavitated facet depends on the magnitude of the applied tensile load as well as the specific material and geometrical characteristics of the polycrystal. At very low applied stress, it is often reasonable to approximate the grains as rigid bodies. The Nabarro–Herring and/or Coble diffusional flow of material between grain boundary facets, driven by chemical potential differences proportional to differences in normal stress, then accommodates local openings at cavitated facets and hence allows overall strain of the polycrystal. At higher applied stresses, the dislocation creep of grain interiors serves as a more responsive accommodation mechanism to grain boundary void growth.

The particular 3-D model used consists of a periodic arrangement of the 14-sided Wigner–Seitz cells of a f.c.c. lattice [see Fig. 4(a,b)]. Particular features

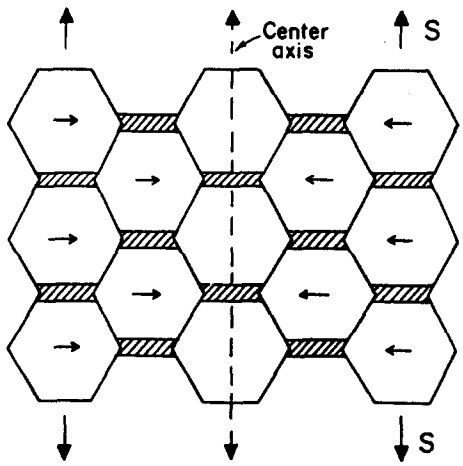

Fig. 3. Widespread cavitation in a 2-D regular hexagonal structure. Grains need not deform to accommodate cavity growth; they need only to displace inward a macroscopic center axis.

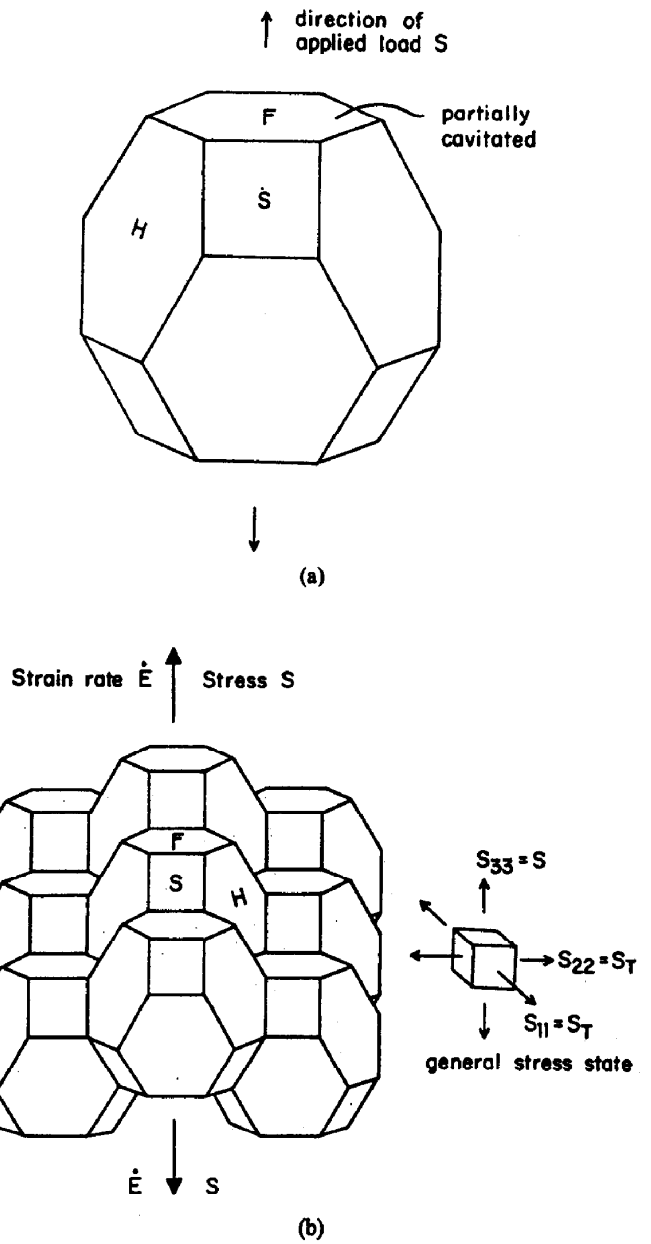

Fig. 4. (a) The Wigner–Seitz cell of an f.c.c. lattice. All faces F are perpendicular to the macroscopic load S and are partially cavitated. Uncavitated faces are either square (S) or hexagonal (H). (b) The periodic assemblage of such cells, subjected to load $S_{33} = S$, with corresponding strain rate $\dot{E}$. The cell boundaries are assumed to slide freely.

of the arrangement are that it completely fills space and has a high degree of symmetry which greatly simplifies analysis. Stress S is applied in a direction normal to a family of hexagonal faces marked F. The limiting case of closely-spaced cavitated facets is represented by specifying all such faces oriented perpendicular to the far-field applied stress S to be cavitated. All grain boundaries are assumed to slide freely. The accompanying macroscopic strain rate in the direction of S is $\dot{E}$. As illustrated, we also consider the possibility of transverse stresses S_T and denote by $\dot{E}_T$ the strain rate in the transverse directions.

ANALYSIS OF ACCOMMODATION BY DISLOCATION CREEP

Here, applied stress levels are assumed high enough for dislocation creep of the grains to be the primary accommodation mechanism for the opening rate $\dot{\delta}$ of the cavitating facets. The analysis is done as now outlined.

(i) *Stress-based variational principle*

A stress-based variational principle is developed in Appendix A for the Wigner–Seitz cell model. Here

the grain material is modeled as linear or nonlinear viscous. We regard the macroscopic stress tensor S_{ij} and stress σ_F on the cavitated facets as "given", and seek to determine, in terms of them, the overall strain rate $\dot{E}_{ij}$ and average opening rate $\dot{\delta}$ of the cavitated facets. The latter relation is analogous to (1). Formulated in Appendix A is an averaged complementary-energy-like density $\Psi(\sigma_{ij})$, defined as a functional of any local stress field σ_{ij} in the cell satisfying:

$\partial\sigma_{ij}/\partial x_j = 0$ (local equilibrium in grain volume)
σ_{ij} produces no shear traction on the grain surface
σ_{ij} equilibrates the given applied stress state S_{ij} [see equation (A4)]
$n_i\sigma_{ij}n_j = \sigma_F$, the given applied load, on the cavitated facet
σ_{ij} produces normal tractions on the grain surface which are consistent with the periodicity of the polycrystal [see condition stated immediately before equation (A4)].

Of all admissible grain stress states satisfying the above, the actual solution renders $\Psi(\sigma_{ij})$ a minimum. The variational principle $\Delta\Psi(\sigma_{ij}) = 0$ produces the strain displacement relations [see relation stated immediately before equation (A5)] and also a compatibility relation between $\dot{E}_{ij}$, $\dot{\delta}$ and the component of velocity normal to the grain surface [see equation (A2)]. The macroscopic strain rate tensor $\dot{E}_{ij}$ and average opening rate $\dot{\delta}$ of the cavitated facet are then given as

$$\dot{E}_{ij} = \frac{\partial \Psi_{\min}}{\partial S_{ij}}, \quad \dot{\delta} = -\frac{V_g}{A_F}\frac{\partial \Psi_{\min}}{\partial \sigma_F}. \tag{2}$$

Here V_g is the grain volume and A_F is the area of the cavitated facet.

(ii) An approximate stress state in the grain

A local stress state σ_{ij} meeting the above conditions may be constructed as the sum of a uniform hydrostatic state $\lambda\delta_{ij}$ and seven uniform uniaxial stress states; each uniaxial field acts only within a right cylindrical column positioned through the grain and defined by one of the set of seven face pairs (see Fig. 5)

$$\sigma_{ij}(\mathbf{x}) = \lambda\delta_{ij} + \sum_{\alpha=1}^{7} [\sigma^{(\alpha)} - \lambda] q^{(\alpha)}(\mathbf{x}) n_i^{(\alpha)} n_j^{(\alpha)}. \tag{3}$$

Here, α is an index for the seven face pairs; $q^{(\alpha)}(\mathbf{x}) = 1$ for $\mathbf{x}$ in column α and $=0$ otherwise; $\mathbf{n}^{(\alpha)}$ is a unit vector along the column generator, and $\sigma^{(\alpha)}$ is the normal stress on the face pairs of column α.

Accordingly, $\Psi(\sigma_{ij})$ can be expressed as the integral over a cell of an algebraic function of λ and the seven $\sigma^{(\alpha)}$. Specifying S_{ij}, σ_F as given determines the seven $\sigma^{(\alpha)}$ and Ψ is minimized with respect to the remaining free parameter λ. Then $\Psi_{\min} = \Psi_{\min}(S_{ij}, \sigma_F)$, and (2) is used assuming an axisymmetric macroscopic stress state $S_{33} = S$, $S_{11} = S_{22} = S_T$ and all other $S_{ij} = 0$. The procedure can be carried out readily for linearly viscous grain creep. In that case the average opening rate $\dot{\delta}$ and strain rates $\dot{E}$ and $\dot{E}_T$ in the directions of S and S_T, respectively, are given by

$$\dot{\delta} \approx 4.33[1.67S - 0.67S_T - \sigma_F]d/\mu \tag{4}$$

$$\dot{E} \approx 3.02[1.85S - 0.85S_T - \sigma_F]/\mu \tag{5a}$$

$$\dot{E}_T \approx -0.61[2.11S - 1.11S_T - \sigma_F]/\mu. \tag{5b}$$

Here, d is the diameter of the cavitated facet and μ is the linear shear viscosity of the material, i.e. $\dot{\varepsilon} = \sigma/3\mu$ for uniaxial tension of a crystallite.

The effect of sliding grain boundaries in an uncavitated, uniaxially loaded specimen ($S_T = 0$) may be estimated by setting $\dot{\delta} = 0$ in (4). We then see that $\sigma_F \approx 1.67S$, which determines the factor β as ≈ 1.67 for the Wigner–Seitz cell geometry. Inserting this value of σ_F into (5a), the macroscopic strain rate is then $\dot{E} \approx 1.63S/3\mu$ (later denoted as $\dot{E}_{\text{nocav}}$). This is as compared to $\dot{E} = S/3\mu$ when there is no grain boundary sliding. By the analogy between linear elastic and linear viscous materials, the same results hold for the Wigner–Seitz model with linear elastic grains of Poisson's ratio $\nu = 1/2$, if the strain rate $\dot{E}$ is replaced by strain E and if μ is regarded as the elastic shear modulus. The ratio of the elastic strain when grain boundary shear tractions are relaxed to that when no relaxation of shear tractions occurs would therefore be 1.63 for loading of the Wigner–Seitz cells in the direction indicated. We compare this value to the theoretical calculations of Zener [15] who obtained a value of approximately 1.32 by applying strain energy considerations to spherical grains.

(iii) Interpretation of μ for nonlinear materials

An extension of the formulation is now made to include nonlinear materials described by the creep rate $\dot{\varepsilon}(\sigma) = [T \text{ dependent factor}] \times \sigma^n$ for which n is the creep exponent. Direct use of the variational formulation is prohibitively complex for that case, so instead we proceed in an approximate manner as indicated in order to have a basis for simple estimates of material response. The local grain strain rate and stress deviatoric tensors are related as

$$\dot{\varepsilon}_{ij} = \frac{1}{2\mu}\tau_{ij} \quad \text{where} \quad \tau_{ij} = \sigma_{ij} - \frac{1}{3}\sigma_{kk}\delta_{ij} \tag{6}$$

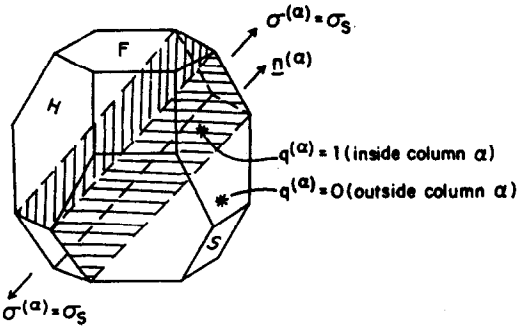

Fig. 5. One of the seven column stress states comprising the approximate local stress state σ_{ij} in the grain.

and the nonlinear viscosity μ is related to the equivalent stress σ_e as

$$\mu = \sigma_e/3\dot{\epsilon}(\sigma_e) \propto \sigma_e^{-(n-1)} \quad \left[\sigma_e^2 = \frac{3}{2}\tau_{ij}\tau_{ij}\right]. \tag{7}$$

We obtain an approximate effective viscosity of the grain, for use in (4) and (5), by using (7) with σ_e being the function of S and σ_F obtained as the square root of the cell average of σ_e^2 for the linear solution described in (ii). Results express this average equivalent stress $\bar{\sigma}_e$ for a tensile loading ($S_T = 0$) as

$$\bar{\sigma}_e(S, \sigma_F) \approx [16.7S^2 - 18.1S\sigma_F + 5.47\sigma_F^2]^{1/2}. \tag{8}$$

Here, $\bar{\sigma}_e$ varies from about 1.3S for $\sigma_F = 1.67S$ to about 4.1S for $\sigma_F = 0$. If (8) is inserted into (7), the ratio of grain-averaged viscosities for a polycrystal with completely cavitated facets (i.e. with all grain boundary cavities coalesced) to that for a polycrystal with no cavitation is

$$\frac{\mu_{\text{complcav}}}{\mu_{\text{nocav}}} \approx \left[\frac{\bar{\sigma}_e(S, 1.67S)}{\bar{\sigma}_e(S, 0)}\right]^{n-1} \sim \frac{1}{(3.1)^{n-1}}. \tag{9}$$

This is a numerically significant effect, and an important aim for further work is the clarification of the accuracy of the somewhat rough approximations adopted here, perhaps by applying directly our variational principle to the nonlinear case.

(iv) Comparison of opposite limiting cases

We can now consider the two limiting cases for which the cavitated facets are *well-separated* and *closely-spaced*, respectively. In the former case, $\dot{\delta}$ is given by (1) using $\alpha = 1.8$ (corresponding to a polycrystal with freely-sliding grain boundaries and a creep exponent $n = 5$), $\beta = 1.67$, and $\dot{E}_{\text{nocav}}$ is given by (5a) by setting $\sigma_F = 1.67S$, $S_T = 0$ and by evaluating $\mu = \mu(S, 1.67S)$. In the latter case, i.e. that for which all facets of type F are cavitating, we use directly (4) and (5a) with $S_T = 0$ and $\mu = \mu(S, \sigma_F)$. Thus, to compare the two limiting cases

$$\left.\begin{aligned}\dot{\delta} &\approx 0.58[1.67S - \sigma_F]d/\mu(S, 1.67S)\\ \dot{E} &\approx \dot{E}_{\text{nocav}} \approx 0.54S/\mu(S, 1.67S)\end{aligned}\right\} \quad \text{(well-separated)} \quad \begin{matrix}\text{(10a)}\\ \text{(10b)}\end{matrix}$$

$$\left.\begin{aligned}\dot{\delta} &\approx 4.33[1.67S - \sigma_F]d/\mu(S, \sigma_F)\\ \dot{E} &\approx 3.02[1.85S - \sigma_F]/\mu(S, \sigma_F)\end{aligned}\right\} \quad \text{(closely-spaced).} \quad \begin{matrix}\text{(11a)}\\ \text{(11b)}\end{matrix}$$

(v) Results for well-constrained and unconstrained void growth

The results discussed herein assume that cavities are present at the initial stage. Hence, the time to nucleate such cavities is not considered. Instead, we focus on the time to rupture, t_r, needed for a uniform distribution of cavities on a facet of type F [see Fig. 4(a)] to grow from an initial cavity radius a_i to a final radius b at coalescence. Thus

$$t_r = \int_{a_i}^{b} \frac{1}{\dot{a}}\, da. \tag{12}$$

Here, $\dot{a}$ is the time rate of change of the cavity radius.

Given a cavity geometry such as that in Fig. 6, $\dot{a}$ may be related to $\dot{\delta}$ through a statement of the conservation of material. Including an as yet unstated relation that characterizes the cavity growth process [i.e. $\dot{\delta} = \dot{\delta}(\sigma_F)$ where the function depends also on b and the current a] enables one to eliminate σ_F from (10a) and (11a), and thus to obtain $\dot{a}$ and t_r as a function of the applied stress S.

For cases where the void growth process is greatly constrained, σ_F may be driven down towards the sintering threshold level σ_0, so that $\sigma_F - \sigma_0 \ll \beta S - \sigma_0$. As will be shown later, such constrained conditions may be realized at sufficiently low S. One can calculate t_r for such strongly constrained conditions. For example, if cavities are assumed to be of a quasi-equilibrium spherical cap shape during growth (see Fig. 6), then conservation of material requires that $\pi b^2\delta = 4\pi h(a^3 - a_i^3)/3$. Here, h depends on the cavity dihedral tip angle and a typical value is $h = 0.6$ (see Chuang *et al.* [5]). Thus, we differentiate with respect to time to obtain

$$\dot{\delta} = 4h(a^2/b^2)\dot{a} \tag{13}$$

Then for $\sigma_F - \sigma_0 \ll \beta S - \sigma_0$, $\dot{\delta}$ for the well-separated and closely-spaced distributions of cavitated facets is given in terms of S and σ_0, by replacing σ_F with σ_0 in (10a) and (11a), respectively. Using (12) and (13), we find

$$\frac{(t_r)_{\text{well-separated}}}{(t_r)_{\text{closely-spaced}}} \approx 7.2\frac{\mu(S, 1.67S)}{\mu(S, \sigma_0)} = 7.2\left[\frac{\bar{\sigma}_e(S, 1.67S)}{\bar{\sigma}_e(S, \sigma_0)}\right]^{n-1} \tag{14}$$

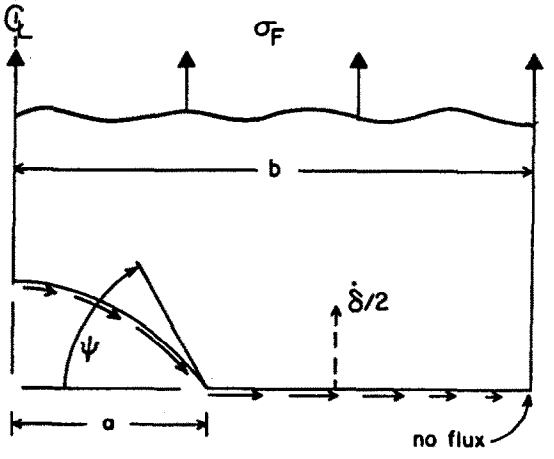

Fig. 6. Axi-symmetric geometry used to analyze cavity growth. Cavities enlarge by surface transport of material to the cavity tip, and subsequent transport of this material by boundary diffusion into the adjoining region between cavities.

where here σ_0 is to be understood as an average as weighted by the integral in (12).

The bracketed ratio in (14) is evaluated for various values of $\sigma_0/1.67S$ by using (8). Assuming $\sigma_0/1.67S \ll 1$, the bracketed ratio is ≈ 3.1 as predicted by (9). For $\sigma_0/1.67S = 0.4$, the bracketed ratio is ≈ 2.0. Thus, it is found for low to moderate values of $\sigma_0/1.67S$ that (14), valid for conditions of strong constraint, predicts a considerably longer time to rupture for the well-separated geometry than for the closely-spaced one. For example, if the material is characterized by a creep exponent of 5, then in the range of $\sigma_0/1.67S$ discussed above, $(t_r)_{\text{well-separated}}$ is of at least two orders of magnitude greater than $(t_r)_{\text{closely-spaced}}$.

Bounds on the total strain to failure may be constructed using (10a,b) and (11a,b) along with an assumption about the cavity shape during growth. By using (10b) to eliminate S from (10a), or equivalently, by considering (1) with $\sigma_F \leq \beta S$, a secluded cavitating facet opens at a rate bounded by $\dot{E}_{\text{no cav}} \times d$, i.e.

$$\dot{\delta}_{\text{well-separated}} \leq \alpha \dot{E}_{\text{no cav}} d. \tag{15}$$

If, for example, cavities are assumed to be of a quasi-equilibrium spherical cap shape during growth, then volume conservation requires the average opening of the cavitated facet at rupture to be $\delta_r = (4h/3)b(1 - f_i^{3/2})$ where $a_i^2/b^2 = f_i$ = initial area fraction of grain boundary which is cavitated. Here, we assume $h = 0.6$. Integrating each side of (15), respectively, from $\delta = 0$, $E = 0$ to $\delta = \delta_r$, $E = E_r$ and setting $\alpha = 1.8$ (corresponding to a polycrystal with freely-sliding grain boundaries and a creep exponent of 5), one obtains

$$(E_r)_{\text{well-separated}} \geq 0.44(b/d)(1 - f_i^{3/2}). \tag{16}$$

A bound on E_r for the closely-spaced situation is constructed in a similar manner; equation (11b) is used to eliminate S in the bracketed term of (11a)

$$\dot{\delta}_{\text{closely-spaced}} \approx \frac{4.33d}{\mu(S, \sigma_F)} \times \left[\frac{1.67\dot{E}\mu(S, \sigma_F)}{(3.02)(1.85)} - \left(1 - \frac{1.67}{1.85}\right)\sigma_F\right]. \tag{17}$$

Since the second term in (17) is inherently positive, a bound is constructed where $\dot{\delta} \leq 1.29\,\dot{E}d$, the equality holding when $\sigma_F = 0$. Integration of (17) as with (15) yields

$$(E_r)_{\text{closely-spaced}} \geq 0.62(b/d)(1 - f_i^{3/2}). \tag{18}$$

The equalities in (16) and (18) hold when constraint is strong, i.e. when $\sigma_F - \sigma_0 \ll \beta S - \sigma_0$ and also $\sigma_0 \ll \beta S$.

In the other limit for which cavity growth is unconstrained, the details of the distribution of cavitated facets become irrelevant when calculating t_r and E_r. Here t_r for any distribution of cavitated facets is determined as the time for cavities on a single facet to coalesce, given that $\sigma_F = \beta S$ (see Fig. 1). One also observes that setting $\sigma_F = \beta S$ in (10b) and (11b) gives $\dot{E}$ as the same for both the well-separated and closely-spaced situations. Since t_r is also the same for both the well-separated and closely-spaced situations, E_r, given here by the product of $\dot{E}$, and t_r, is unchanged as well. Hence, the proximity of cavitated facets to one another does not change greatly the total strain to rupture, but it does alter the time to rupture substantially, at least when cavity growth is greatly constrained.

For the closely-spaced geometry, the contribution of the void growth process to the total strain may be estimated as the opening of the cavitated facet at coalescence divided by the separation distance between two grain centers. Using a quasi-equilibrium spherical cap cavity shape, one estimates this contribution to be $0.59(b/d)(1 - f_i^{3/2})$ as compared to the estimate for E_r in (18). Hence for the closely-spaced situation under constrained conditions, the void growth process is seen to be a major contributor to the total rupture strain. This last observation is supported by Harris *et al.* [16] and Hanna *et al.* [17] whose long term fracture experiments showed that the volumetric strain may become the dominant strain.

VOID GROWTH BY THE HULL-RIMMER PROCESS

Bounds on E_r have been constructed for the limiting cases of completely constrained and completely unconstrained void growth. The stress and temperature regimes for which constraint is actually important are obtained by characterizing the void growth process (i.e. expressing $\dot{\delta}$ as a function of σ_F) and coupling results with (10) and (11).

A basic model for grain boundary void growth was proposed by Hull and Rimmer [1]. Here, cavities enlarge by surface transport of material to the cavity tip, and subsequent transport of this material by diffusion into the adjoining grain boundary region between two cavities (Fig. 6). Boundary diffusion is normally the dominant transport process and then the resulting opening rate of the cavitating facet is given in [9] as

$$\dot{\delta} = \frac{4\mathcal{D}_b}{b^2} \frac{[\sigma_F - 2(1-f)(\gamma_s/a)\sin\psi]}{[ln(1/f) - (3-f)(1-f)/2]}. \tag{19}$$

Here $\mathcal{D}_b = D_b\delta_b\Omega/kT$ as explained earlier; γ_s is a surface energy, ψ is the cavity tip dihedral angle and $f = a^2/b^2$ is the voided area fraction. The void half spacing b is assumed to be uniform over position and time in this calculation although in actuality, nucleation effects may make cavity spacing a function of time and of the relative orientation of grains joining at a facet. The bracketed term in the denominator is solely a function of the current voidage fraction f and it is of order unity for typical f values. The term subtracted from σ_F represents a sintering cutoff stress $\sigma_0 = 2(1-f)(\gamma_s/a)\sin\psi$ which is frequently negligible compared to βS.

In the Hull–Rimmer analysis, cavities are assumed to retain a quasi-equilibrium spherical cap shape. This is valid for low $\dot{a}$ and low σ_F, or equivalently, when the rate of material transport by surface diffusion greatly exceeds that due to boundary transport [5, 18]. In addition, $\dot{\delta}$ is assumed to be independent of position along the cavitated facet. This is valid [9, 18, 19, 20] for $a + 1.5\tilde{L} \geq b$, where the length parameter $\tilde{L} = [\mathcal{D}_b\sigma_F/\dot{\epsilon}(\sigma_F)]^{1/3}$ is defined as is L, except that it is based on σ_F rather than the applied stress S. An interpretation is that the matter diffused from the cavity is accommodated nonuniformly on the grain boundary, with local creep flow allowing openings to occur only over a distance of order $\tilde{L}$ ahead of the cavity tip. From this observation, Chen and Argon [19] suggest a reasonable approximation to the finite element results of Needleman and Rice [9] for the case of tensile loading is to use (19), but with f replaced by the maximum of $(a/b)^2$ and $\{a/(a+\tilde{L})\}^2$. Work by Sham and Needleman [20] suggests a best fit of this approximate method to the data is obtained if a factor of 1.5 multiplying $\tilde{L}$ is inserted into the above formula for f. Equation (19) may be altered to account for other effects; for instance, the influence of triaxiality on cavity growth rate could be included in the present analysis by adopting an approximate expression given by Sham and Needleman [20] rather than use (19).

Use of (19) to eliminate σ_F from (10a) and (11a) gives the opening rate, $\dot{\delta}$, for the well-separated and closely-spaced geometries in terms of the applied stress S. In particular, the opening rate normalized with that when no constraint exists (i.e. $\sigma_F = 1.67S$) gives for the well-separated case

$$\frac{\dot{\delta}}{(\dot{\delta})_{\sigma_F=1.67S}} = \frac{\sigma_F - \sigma_0}{1.67S - \sigma_0} \approx \frac{[\ln(1/f) - (3-f)(1-f)/2]}{[2.2L^3/b^2d] + [\ln(1/f) - (3-f)(1-f)/2]}. \quad (20)$$

The degree of constaint is determined by comparison of the two bracketed terms in the denominator of (20). Constraint is important when the first of the bracketed terms in the denominator is comparable to or greater than the second of the bracketed terms or equivalently, when L^3/b^2d is of order unity or greater (since the second of the bracketed terms in the denominator is of order unity).

As mentioned, L decreases with increasing stress and temperature. Needleman and Rice [9] observe that when power-law creep occurs with an activation energy equal to that for bulk (lattice) diffusion, L may be expressed as $L(S) = L_0 \exp(\kappa T_m/T)(10^{-3}G/S)^{(n-1)/3}$ where L_0 and κ are constants, T_m is the absolute melting temperature, n is the creep exponent and G is the elastic shear modulus. They find that for $S = 10^{-3}G$ and $T = 0.5\,T_m$, L ranges from about 2 to 8 μm for some common f.c.c. metals and from about 0.25 to 0.35 μm for some b.c.c. metals [9]. For $S = 10^{-4}G$ at the same temperature, the above values are increased by about a factor of 20. Increases in temperature, for example from $0.5\,T_m$ to $0.8\,T_m$, decrease L by a factor between 0.05 and 0.28, depending on the material, for fixed S/G. Hence, the constraint effect decreases with increasing applied stress and temperature.

A similar expression for the closely-spaced situation states

$$\frac{\dot{\delta}}{(\dot{\delta})_{\sigma_F=1.67S}} = \frac{\sigma_F - \sigma_0}{1.67S - \sigma_0} \approx \frac{[\ln(1/f) - (3-f)(1-f)/2]}{[0.3L^3(S/\bar{\sigma}_e)^{n-1}/b^2d] + [\ln(1/f) - (3-f)(1-f)/2]}. \quad (21)$$

Again, constraint is measured by comparison of the two bracketed terms in the denominator. Comparing (21) to (20) the effect of having closely-spaced cavitated facets is seen to reduce the first of the bracketed terms, first by the smaller factor of 0.3 and second, by the introduction of the factor $(S/\bar{\sigma}_e)^{n-1}$, which ranges from $(1/1.3)^{n-1}$ for $\sigma_F = \beta S$ to $(1/4.1)^{n-1}$ for $\sigma_F = 0$. The constraint effect is thus reduced as cavitated facets become closely-spaced. As will be seen in a later example, it is typically significant even then at low applied stress.

Cocks and Ashby [12] obtained an approximate expression for $(\sigma_F - \sigma_0)/(1.67S - \sigma_0)$ as a function of the spacing, $2l$, of cavitated facets of size d. Their result is similar in form to (20, 21) where the degree of constraint is measured by comparison of two terms in the denominator. In particular, their result is obtained by replacing the factor of 2.2 in (20) by $(16/3)(1 - d/2l)^n$ and by multiplying the second of the bracketed terms in the denominator of (20) by $[1-(1-d/2l)^n]$. In the limits of $(d/2l) \ll 1$ and $(d/2l) = 1$, the Cocks and Ashby result agrees qualitatively with the respective expressions for the well-separated and closely-spaced situations discussed here, in that well-separated conditions rather than more closely-spaced ones favor constrained cavity growth.

Work by Dyson *et al.* [21] and Raj [22] has considered the effect of constrained cavity growth in altering the macroscopic behavior of damaged material. In particular, Dyson *et al.* subjected 20/25/Nb stainless steel to a multiple-mechanical-thermal-treatment which increases the amount of grain boundary cavitation and observed that the macroscopic deformation rate could no longer be described by the applied effective stress as in classical plasticity theory, but rather that a dependence on hydrostatic pressure be included as well.

This observation may be studied within the closely-spaced analysis presented here by using (4,5a) with μ interpreted as a grain-averaged viscosity as discussed earlier. Setting the opening rate of the cavitating facet, $\dot{\delta}$, in (4a) equal to that predicted by a Hull–Rimmer cavity growth model in (19) yields a

relation between σ_F, S and S_T. Combining this relation with (5a) gives

$$\dot{E} \approx 3[(1-\eta)S + (0.85 - 0.67\eta)(S - S_T)]/\mu \quad (22)$$

where $\eta = \sigma_F/[S + 0.67(S - S_T)]$ is given by the right-hand side of (21) when the sintering cutoff is neglected, and is a measure of to what degree cavity growth is constrained. Here, $\eta = 1$ implies no constraint of the cavity growth process, whereas $\eta = 0$ implies strong constraint. The explicit dependence of μ on the applied stress state is obtained by using (7) with a generalized version of (8) for a biaxial stress state, and this is

$$\bar{\sigma}_e \approx [(5.5\eta^2 - 10.9\eta + 5.4)S^2 + (7.3\eta^2 - 14.5\eta + 7.2)S(S - S_T) + (2.5\eta^2 - 4.9\eta + 4.1)(S - S_T)^2]^{1/2} \quad (23)$$

(which means that η is determined implicitly by equation 21). Hence, we see that $\dot{E}$ for closely-spaced conditions with little or no constraint ($\eta \approx 1$), like $\dot{E}$ for a well-isolated geometry, depends only on $S - S_T$ as would be observed in classical plasticity theory. However, for closely-spaced geometries where cavity growth is greatly constrained ($\eta \ll 1$), $\dot{E}$ depends on both the maximum principal stress S and $S - S_T$ (and increasingly so on S as the cavity growth becomes more constrained). These basic features agree qualitatively with the studies presented in [21, 22].

NUMERICAL RESULTS FOR PURE NICKEL

Given specific values of f, b, d, S and the necessary physical parameters to determine $L(S)$, then equations (21) and (11a) for the closely-spaced situation or (20) and (10a) for the well-separated case are a pair of equations containing two unknown parameters $\dot{\delta}$, σ_F. One may then solve for σ_F and $\dot{\delta}$ and thus obtain $\dot{a}$ by using (13). Equation (12) is then used to determine t_r.

Considered here is a pure nickel polycrystal of the Wigner–Seitz cell geometry discussed, loaded in uniaxial tension S. Cavities are located on grain boundary facets oriented perpendicular to the applied stress, and they are assumed to grow by a Hull–Rimmer diffusive growth mechanism that is modified by the approximate method of Chen and Argon [19] described earlier. The opening of such cavitated facets is accommodated by the nonlinear creep of grains, the boundaries of which are freely-sliding. For the results illustrated, the cavity half-spacing b and facet diameter d are 1.3 and 50 μm, respectively, where the initial void size a_i is taken as 0.13 μm.

The parameter L, which characterizes the diffusional and dislocation creep properties of the material is defined as earlier in terms of the constants L_0 and κ, the melting temperature T_m, creep exponent n and elastic shear modulus G. For nickel, Needleman and Rice [9] tabulate $L_0 = 2.57 \times 10^{-3}$ μm, $\kappa = 3.90$, $T_m = 1726$K, $n = 4.6$ and G is estimated to be 8.1×10^4 MPa. The resulting values of L are regarded as representative of other pure f.c.c. metals. Here, an estimate $\gamma_s = 1.725$ J/m^2 for the surface energy of nickel is used from Chuang *et al.* [5].

The time to rupture is calculated as described earlier, using (12). Figure 7(a) shows t_r vs S/G at $T = 0.5\,T_m$ for each of the opposite limiting cases of well-separated and closely-spaced cavitated facets as compared to the unconstrained situation for which $\sigma_F = 1.67S$. For applied loads greater than about $3 \times 10^{-3}G$, values of t_r on the order of minutes are predicted. Here, cavity growth is unconstrained and t_r based on $\sigma_F = 1.67S$ provides a good estimate of the actual time to rupture.

For applied loads less than about $1 \times 10^{-3}\,G$, the void growth process is indeed constrained and times to rupture for the well-separated and closely-spaced situations are many times larger than t_r based on $\sigma_F = 1.67S$. In this constrained regime, the proximity of cavitated facets to one another (bounded here by the well-separated and closely-spaced extremes) is seen to vary t_r by up to two orders of magnitude. Thus, we find here that $(t_r)_{\text{well-separated}} \gg (t_r)_{\text{closely-spaced}}$.

Also apparent in the well constrained regime is that t_r for the well-separated and closely-spaced geometries is dependent on S^{-n}. This occurs since for constrained conditions, the dependence of t_r on S is determined by the features of the accommodation mechanism, given here as the power-law creep of grains. In particular, the cavity growth rate is determined by using (13) and also (10a), (11a) for the well-separated and closely-spaced geometries, respectively, evaluating σ_F approximately as the sintering threshold. The resulting cavity growth rates are dependent on applied stress as S/μ, which is

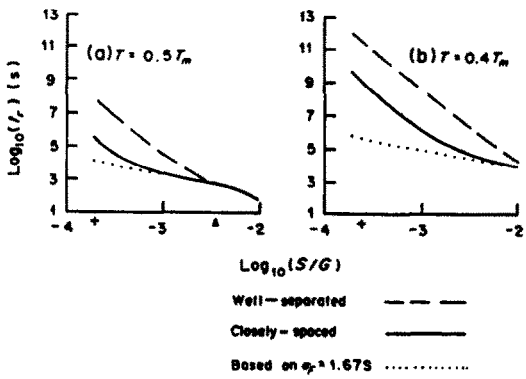

Fig. 7. Time to rupture t_r of pure nickel versus normalized applied load S/G (G = elastic shear modulus) for the cases of well-separated and closely-spaced cavitated facets, and for that based on $\sigma_F = 1.67S$. Results are for temperatures (a) $T = 0.5T_m$ and (b) $T = 0.4\,T_m$. In each case, cavity half spacing $b = 1.3$ μm, cavitated facet diameter $d = 50$ μm, and initial cavity size $a_i = b/10$. Local creep flow on cavitating boundaries aids the diffusive rupture process for applied loads greater than (△). For applied loads less than (+), Nabarro–Herring and/or Coble creep are expected to be more responsive accommodation mechanisms than the dislocation creep of grains assumed here.

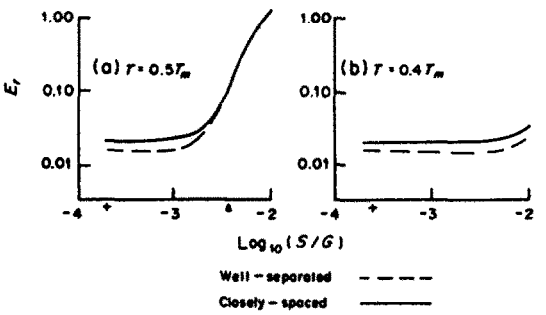

Fig. 8. Strain to rupture E_r of pure nickel versus normalized applied load S/G for the well-separated and closely-spaced geometries of cavitated facets. Results are for temperatures (a) $T = 0.5\,T_m$ and (b) $T = 0.4\,T_m$. Values of b, d, a_i and the meanings of (△), (+) are the same as in Fig. 7.

proportional to S^n. The time to rupture is then calculated using (12), so that t_r is dependent on S^{-n}.

At an applied load S equal to about $2 \times 10^{-4}\,G$, the load carried across the cavitated facet equals approximately the sintering stress limit based on the initial cavity size. Cavity growth is then negligible and times to rupture for each of the three cases plotted in Fig. 7(a) asymptotically approach infinity. Since the sintering stress depends on the inverse of the cavity radius, the sintering threshold is strongly dependent on the initial cavity radius a_i. For instance, if a_i is increased from the value of 0.13 μm in Fig. 7a to 0.5 μm, the sintering threshold would be decreased by about four times.

A lower limit of applied load to the validity of this analysis is shown on the abscissa of Fig. 7(a). Below this, Nabarro–Herring and/or Coble creep is expected to act as a more responsive accommodation mechanism than the power-law creep of grains considered here. This latter estimate of S/G is made using deformation maps [23] for a pure nickel polycrystal of grain size 100 μm, and at $T/T_m = 0.5$. An upper value of the applied load is also set (based on [9, 19, 20] and $\dot{L}$ as discussed earlier), above which local creep flow between cavities on a boundary shortens the necessary diffusive path length for cavity growth.

The effect of temperature on rupture time is observed by comparing Fig. 7(a) (where $T = 0.5\,T_m$) and Fig. 7(b) (where $T = 0.4\,T_m$). Here, a temperature decrease substantially increases predictions for t_r, more so for the well-separated and closely-spaced geometries, but also for that based on $\sigma_F = 1.67S$. Accompanying these increases in t_r are increases in the ranges of S/G over which cavity growth is constrained.

The total strain to rupture is calculated according to

$$E_r = \int_{a_i}^{h} \frac{\dot{E}}{\dot{a}}\,da. \tag{24}$$

Figures 8(a, b) show E_r to be relatively unchanged by the proximity of cavitated facets to one another as predictions of E_r for the well-separated and closely-spaced geometries differ little. The lower shelf of each plot corresponds to a strong constraint regime and each shelf spans a rather large range of applied stress. Values of E_r in this range agree well with the lower bounds developed earlier as (16), (18). The strain to rupture increases rapidly from the shelf as the constraint effect becomes less important.

Rice [11] considers the limiting situation in which cavitated facets are well-separated and observes that cavity growth rate is proportional to $\dot{E}_{\text{nocav}}$ for conditions of strong constraint. Thus, it is under such constrained conditions that his results are compatible with a Monkman–Grant [24] correlation (i.e. $\dot{E}_{\text{nocav}} t_r$ is approximately constant), and t_r may be estimated by determining $\dot{E}_{\text{nocav}}$.

Results indicate that a Monkman–Grant correlation may also exist when cavitated facets are closely-spaced. Shown in Fig. 9(a) (where $T = 0.5\,T_m$) and Fig. 9(b) (where $T = 0.4\,T_m$) are plots of $\dot{E}/\dot{E}_{\text{nocav}}$ vs t/t_r for several values of applied load on nickel, assuming the limiting case of closely-spaced cavitating facets. Material and geometrical parameters used here have the same values as stated earlier for Fig. 7(a,b). The initial transient strain rates present in such a creep test are assumed to relax early in the specimen life; they are not considered explicitly here. The upper and lower bounds to strain rate are given as $\dot{E} = \dot{E}_{\text{complcav}}$ (corresponding to $\sigma_F = 0$) and $\dot{E} = \dot{E}_{\text{nocav}}$ (corresponding to $\sigma_F \approx 1.67S$), respectively. As applied load levels become large, cavity growth becomes unconstrained and $\dot{E}$ approaches a steady state value of $\dot{E}_{\text{nocav}}$ [see Fig. 9(a)]. The product $\dot{E}_{\text{nocav}} t_r$ then models E_r well, but as seen in Fig. 8(a), E_r is not constant in this unconstrained cavity growth regime and a Monkman-Grant correlation does not hold.

Conversely, when applied load is decreased, cavity growth may become strongly constrained and $\dot{E}$ may approach a steady state value of $\dot{E}_{\text{complcav}}$ [e.g. see Fig. 9(b)]. The product $\dot{E}_{\text{complcav}} t_r$ then models E_r well, and in Fig. 8(b) it is seen that E_r is relatively constant in this constrained cavity growth regime. Consequently, results for closely-spaced cavitated facets are compatible with Monkman–Grant correlations, at least for the strongly constrained conditions shown in Fig. 9(b). As demonstrated in Fig. 9(a), Monkman-Grant products are not always applicable, even as the applied load is decreased. Here, for $(S/G) \times 10^4 = 2$, the effect of the sintering threshold is seen to vary the creep rate so that a steady state value $\dot{E} = \dot{E}_{\text{complcav}}$ is not achieved. In fact, $\dot{E}$ for most levels of applied load is shown to vary substantially with time, rather than achieve a steady state value, for the limiting case considered of closely-spaced cavitating facets. By comparison, of course, $\dot{E}$ is relatively constant with time for well-separated cavitating facets.

CONCLUSIONS

Constraints as identified by Dyson [10] on the creep cavitation of grain boundary facets are dis-

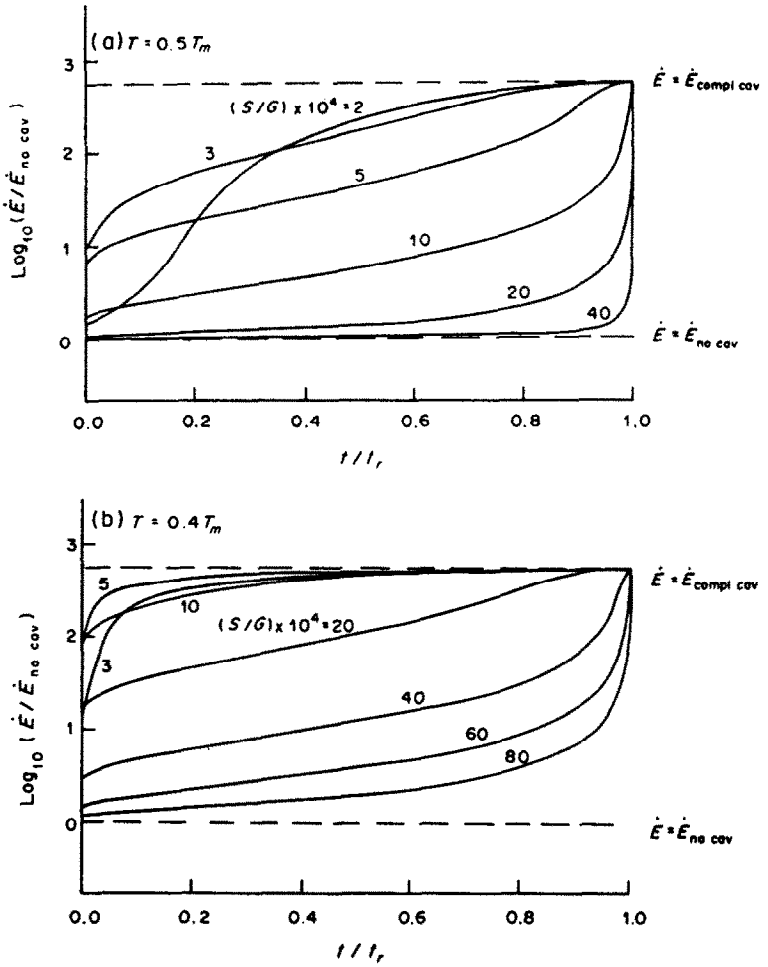

Fig. 9. Normalized strain rate $\dot{E}/\dot{E}_{no\,cav}$ of pure nickel versus normalized time t/t_r for several values of applied load, where (a) $T = 0.5\,T_m$ and (b) $T = 0.4\,T_m$. Values of b, d and a_i are the same as for Fig. 7.

cussed for two opposite limiting cases, the first for well-separated cavitated facets and the other for closely-spaced cavitated facets. These limiting cases are assumed to bound practical situations. The former case was studied by Rice [11] and the latter is analyzed in this paper utilizing a three-dimensional periodic array in which grain boundaries are freely-sliding and all facets oriented perpendicular to a uniaxial load are cavitating.

Comparisons are made between the two limiting cases, assuming that grains creep in a nonlinear manner and thereby accommodate diffusive grain boundary void growth. Results show that the time to rupture, at least of a cavitating facet, is highly dependent on the proximity of cavitated facets to one another. When accommodation is by dislocation creep, the ratio of the times to rupture of the well-separated to the closely-spaced situations ranges from about 50 for a creep exponent $n = 3$ to about 500 for $n = 5$.

Rupture strains, however, are relatively independent of the proximity of cavitated facets to one another. When cavity growth is greatly constrained, E_r may have small and relatively constant values with load and temperature. For such conditions, the rupture strain is directly proportional to b/d, the cavity half-spacing divided by the facet diameter d.

Monkman–Grant correlations are shown to exist for both well-separated and closely-spaced geometries when constraint is strong, or effectively, when applied loads are small. For the well-separated case under such constrained conditions, the product of rupture time and strain rate of an uncavitated polycrystal is found to approximate E_r and therefore to be relatively constant with changing load and temperature. For the closely-spaced situation with strongly constrained cavity growth, the product of rupture time and strain rate of a polycrystal with completely coalesced cavities may be found to approximate E_r and to be relatively constant with load and temperature. However, in this latter limiting case, the cavitation process itself contributes substantially to the total strain.

When cavity growth occurs according to a

Hull–Rimmer model, criteria are obtained for when constraint is dominant or not. For the well-separated case in which the opening of cavitated facets is accommodated by the dislocation creep of grains, constraint is important when the length parameter $L \gtrsim (b^2 d)^{1/3}$; L decreases with increasing applied stress and temperature so that constraint plays a greater role with decreasing temperature and applied stress. When cavitated facets are closely-spaced, constraint is estimated to be strong for L values approximately a factor of 100–1000 times larger than those required for constraint in the well-separated case. The exact factor depends on the creep exponent n and the value of stress across the cavitated facet, although in general, cavity growth is less constrained as cavitated facets become more closely-spaced. As shown, constraint of void growth may be strong even for this closely-spaced geometry.

It remains for future work to bridge the gap between the well-separated and closely-spaced limiting situations discussed here. As a contribution, Appendix B briefly presents results for a closely-spaced situation where the cavitating facets are square faces of the Wigner–Seitz cells, about 40% of the area of the hexagonal facets discussed in the body of the paper.

The heterogeneity of the creep cavitation process also needs to be considered in future work. Cavities are neither spaced uniformly on facets nor are facets themselves spaced uniformly. Recent work by Tvergaard [25] considers the influence of nonuniform initial cavity radii and spacings. It is found that differences in initial cavity radii are quickly evened out when $a_i/\bar{L}$ values are small or equivalently, when matter diffused from the cavities is distributed uniformly on the grain boundary. Further analyses may also include cavity half-spacing as well as the size and proximity of cavitated facets to be a function of time and position.

Acknowledgement—The research was supported by the NSF Materials Research Laboratory at Harvard University.

REFERENCES

1. D. Hull and D. E. Rimmer, *Phil. Mag.* **4**, 673 (1959).
2. M. V. Speight and J. E. Harris, *Metals Sci.* **1**, 83 (1967).
3. J. Weertman, *Metall. Trans.* **5**, 1743 (1974).
4. R. Raj and M. F. Ashby, *Acta metall.* **23**, 653 (1975).
5. T.-J. Chuang, K. I. Kagawa, J. R. Rice and L. Sills, *Acta metall.* **27**, 265 (1979).
6. B. F. Dyson, *Can. Metall. Q.* **18**, 31 (1979).
7. W. Beere and M. V. Speight, *Metals Sci.* **12**, 172 (1978).
8. G. H. Edward and M. F. Ashby, *Acta metall.* **27**, 1505 (1969).
9. A. Needleman and J. R. Rice, *Acta metall.* **28**, 1315 (1980).
10. B. F. Dyson, *Metals Sci.* **10**, 349 (1976).
11. J. R. Rice, *Acta metall.* **29**, 675 (1981).
12. A. C. F. Cocks and M. F. Ashby, *Prog. Mater. Sci.* **27**, 189 (1982).
13. M. He and J. Hutchinson, *Trans. ASME, J. appl. Mech.* **48**, 830 (1981).
14. R. Raj and A. K. Ghosh, *Metall. Trans.* **12A**, 1291 (1981).
15. C. Zener, *Phys. Rev.* **60**, 906 (1941).
16. J. E. Harris, M. O. Tucker and G. W. Greenwood, *Metals Sci.* **8**, 311 (1974).
17. M. D. Hanna and G. W. Greenwood, *Acta metall.* **30**, 719 (1982).
18. J. R. Rice, in *Three-Dimensional Constutive Relations and Ductile Fracture* (edited by S. Nemat-Nasser), p. 173. North-Holland, Amsterdam (1981).
19. I.-W. Chen and A. S. Argon, *Acta metall.* **29**, 1759 (1981).
20. T.-L. Sham and A. Needleman, *Acta metall.* **31**, 919 (1983).
21. B. F. Dyson, A. K. Verma and Z. C. Szkopiak, *Acta metall.* **29**, 1573 (1981).
22. R. Raj, *Acta metall.* **31**, 29 (1983).
23. H. Frost and M. Ashby, in *Deformation-Mechanism Maps: The Plasticity and Creep of Metals and Ceramics*, p. 22. Pergamon Press, Oxford (1982).
24. F. C. Monkman and N. J. Grant, *Proc. Am. Soc. Test. Mater.* **56**, 593 (1956).
25. V. Tvergaard, *J. Mech. Phys. Solids* **32**, 373 (1984).
26. F. Ghahremani, *Int. J. Solids Struct.* **16**, 825 (1979).

APPENDIX A

A solution method for periodic cells via a stress-based variational principle

The variational principle used here is developed from conditions of equilibrium and compatiblity which must be satisfied by the true stress and displacement fields, respectively. These conditions are discussed below:

The grains of a polycrystal are represented by a periodic arrangement of 3-D cells with freely-sliding boundaries between them. Since identical boundary conditions exist on each cell, focus is made on a single cell, in this case a Wigner–Seitz cell of which Fig. A1 shows a cross-sectional cut. Here, the cell is bounded by three pairs of like faces, of which those labelled F are cavitating.

As pointed out by Ghahremani [26], deformation compatibility in a periodic array of cells enforces the continuity of normal displacement across the boundaries of adjoining grains. A macroscopic strain tensor E_{ij} is defined such that the relative displacements of two grain centers separated by

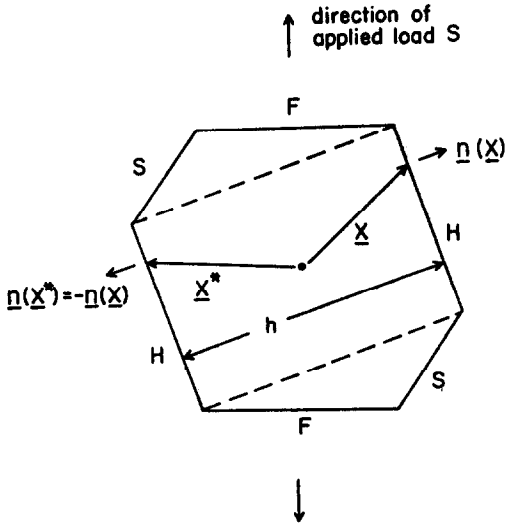

Fig. A1. Cross-sectional cut through Wigner–Seitz cell, showing the three types of face pairs. The dotted lines represent the cylindrical volume of a hexagonal face pair.

the vector D_j is given by $E_{ij}D_j$. Define $u_i(\mathbf{x})$ as the displacement with respect to the grain center of a point with position vector x from the grain center. Hence, the relative displacement vector $\delta_i(\mathbf{x})$ across a grain interface at a point x is given as

$$\delta_i(\mathbf{x}) = E_{ij}hn_j(\mathbf{x}) + u_i^*(\mathbf{x}) - u_i(\mathbf{x}) \tag{A1}$$

Here, $n_i(\mathbf{x})$ is the normal to the grain face containing x and $u_i^*(\mathbf{x}) = u_i(\mathbf{x}^*)$ where $\mathbf{x}^* = \mathbf{x} - h\mathbf{n}(\mathbf{x})$ (see Fig. A1). The actual opening gap $\delta(\mathbf{x})$ at an interface is given by $\delta(\mathbf{x}) = n_i(\mathbf{x})\delta_i(\mathbf{x})$. Defining $u_n(\mathbf{x}) \equiv n_i(\mathbf{x})u_i(\mathbf{x})$ and $u_n^*(\mathbf{x}) = u_n(\mathbf{x}^*) = n_i(\mathbf{x}^*)u_i(\mathbf{x}^*) = n_i(\mathbf{x}^*)u_i^*(\mathbf{x})$ we obtain

$$\delta(\mathbf{x}) = hn_i(\mathbf{x})E_{ij}n_j(\mathbf{x}) - u_n(\mathbf{x}) - u_n^*(\mathbf{x}) \tag{A2}$$

δ vanishes on the noncavitating facets, since here we neglect Nabarro–Herring and Coble creep.

Analogous to E_{ij}, a macroscopic stress tensor S_{ij} is defined in terms of the local stress state σ_{ij}. This local state is assumed to satisfy equilibrium, $\sigma_{ij,j} = 0$, and is related to S_{ij} by

$$S_{ij} = \frac{1}{V_g}\int_{V_g}\sigma_{ij}\,dV = \frac{1}{V_g}\int_{S_g} n_k\sigma_{ki}x_j\,dS. \tag{A3}$$

Here V_g and S_g are the grain volume and surface, respectively. The assumption of vanishing shear on the grain boundary implies $n_k\sigma_{kl} = \sigma(\mathbf{x})n_l$, where $\sigma(\mathbf{x}) = n_in_j\sigma_{ij}$ is the traction normal to the boundary. We use also a result from the periodicity of cell arrangement that $\sigma(\mathbf{x}) = \sigma(\mathbf{x}^*)$ so that (A3) becomes

$$S_{ij} = \frac{1}{2V_g}\int_{S_g} h\sigma n_i n_j\,dS. \tag{A4}$$

The following form of the Principle of Virtual Work then applies for any equilibrium stress field $\{S_{ij}, \sigma_{ij}, \sigma\}$ and any compatible deformation field $\{E_{ij}, \varepsilon_{ij}, \delta, u_i\}$. Equilibrium stress fields are understood to satisfy $\sigma_{ij,j} = 0$, to satisfy (A4), to produce no shear traction on the grain face and to meet $\sigma(\mathbf{x}^*) = \sigma(\mathbf{x})$. Compatible fields are such that $2\varepsilon_{ij} = (u_{i,j} + u_{j,i})$ and that (A2) is satisfied. For any such pair of fields

$$V_gS_{ij}E_{ij} - \frac{1}{2}\int_{S_g}\sigma\delta\,dS = \int_{V_g}\sigma_{ij}\varepsilon_{ij}\,dV. \tag{A5}$$

It can be shown that the validity of (A5) for arbitrary equilibrium fields implies that the deformation field is compatible. Similarly, the validity of (A5) for arbitrary compatible fields implies that the stress field satisfies equilibrium.

A functional of the local stress field σ_{ij} may be defined in a manner analogous to that for the "complementary energy" in elasticity

$$\Psi(\sigma) = \frac{1}{V_g}\int_{V_g}\psi(\sigma)\,dV \quad \text{where} \quad \psi(\sigma) = \int_0^{\sigma}\dot{\varepsilon}_{ij}(\sigma)\,d\sigma_{ij} \tag{A6}$$

and $\dot{\varepsilon}_{ij} = \dot{\varepsilon}_{ij}(\sigma)$ denotes a viscous constitutive relation, consistent with ψ being a function of σ only. The functional is defined on the class of equilibrium stress fields. If the grain material is linear viscous, then $\psi(\sigma) = 1/2\,\sigma_{ij}\dot{\varepsilon}_{ij}$. The infinitesimal variation $\Delta\Psi$ of $\Psi(\sigma)$, associated with variation $\Delta\sigma_{ij}$ of the stress field, is

$$\Delta\Psi(\sigma) = \frac{1}{V_g}\int_{V_g}\dot{\varepsilon}_{ij}(\sigma)\Delta\sigma_{ij}\,dV. \tag{A7}$$

It then follows from the Principle of Virtual Work that for given S_{ij} and stress σ_F on cavitating facets, the true stress field σ_{ij} (namely that equilibrium field σ_{ij} for which the resulting strain rates $\dot{\varepsilon}_{ij} = \dot{\varepsilon}_{ij}(\sigma)$ are compatible) satisfies $\Delta\Psi = 0$. In fact, Ψ is a minimum at the true solution for given S_{ij} and σ, and for variations in these quantities, Ψ_{min} satisfies

$$\Delta\Psi_{min}(\sigma) = \dot{E}_{ij}\Delta S_{ij} - \frac{1}{2V_g}\int_{S_g}\dot{\delta}\Delta\sigma\,dS. \tag{A8}$$

For the particular Wigner–Seitz cell geometry discussed, the opening δ between grain faces is nonzero on the cavitating face denoted here by subscript "F". Approximating σ on face F as uniform and equal to σ_F, (A8) then states

$$\Delta\Psi_{min}(\sigma) = \dot{E}_{ij}\Delta S_{ij} - \frac{A_F}{V_g}\dot{\bar{\delta}}\,\Delta\sigma_F. \tag{A9}$$

Here, A_F is the area of a cavitated face, and $\dot{\bar{\delta}}$ is the average opening of a cavitated facet.

In summary, $\Psi(\sigma)$ is defined in (A6) as a functional of any local stress field σ_{ij} in the grain satisfying the various attributes enumerated in section (i). Among all such equilibrium fields $\{S_{ij}, \sigma_{ij}, \sigma\}$, the exact solution to the problem of prescribed S_{ij} and σ_F renders $\Psi(\sigma)$ a minimum. This value, Ψ_{min}, is a function of the given quantities S_{ij} and σ_F, and it then follows from (A9) that the overall strain rates and average opening rate of the cavitating facets are given by (2).

APPENDIX B

An alternative representation of closely-spaced cavitated facets

The Wigner–Seitz cell model may be oriented in a second manner where square rather than hexagonal faces are normal to a uniaxial stress S and are cavitating (Fig. B1). In this case, the area of cavitated facets is reduced by about 60% over that in the original orientation, but closely-spaced conditions still prevail since each grain contains substantial cavitation.

The development of expressions for $\dot{\delta}$, $\dot{E}$, t, and E, for this second orientation of the Wigner–Seitz cell is identical to that presented for hexagonal cavitated facets. As assumed earlier, the opening of cavitated facets is accommodated by the dislocation creep of grains, grain boundaries slide freely, and cavities are assumed to enlarge by a Hull–Rimmer diffusive growth process. The stress-based variational prin-

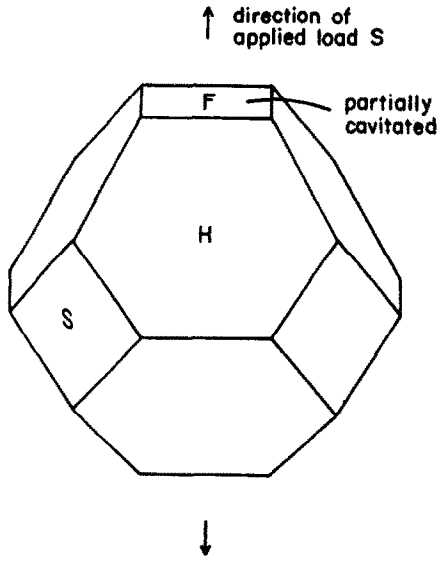

Fig. B1. A second orientation of the Wigner–Seitz cell to the macroscopic applied load S, in which partially cavitated facets are square rather than hexagonal.

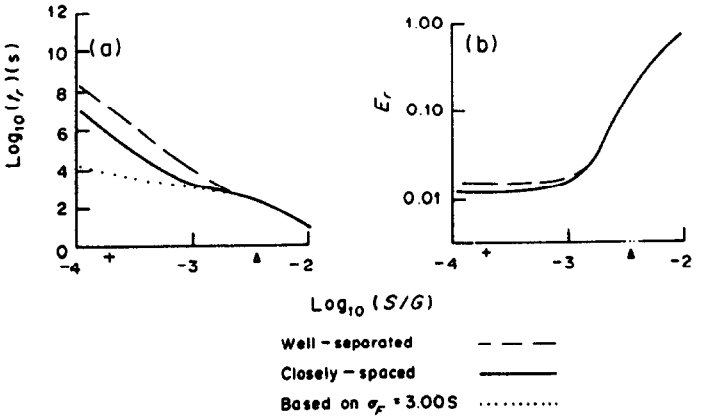

Fig. B2. (a) Time to rupture t_r of nickel vs normalized applied load S/G using the second orientation of the Wigner–Seitz cell in Fig. B1. Here $T = 0.5\,T_m$, $b = 1.3\,\mu$m, $d = 50\,\mu$m and $a_i = b/10$ as in Fig. 7(a). (b) Corresponding strain to rupture E_r vs normalized applied load S/G. Both ($\triangle$) and (+) have the same meanings as in Fig. 7.

ciple described earlier is used, with the approximate stress state defined by (3). For the axisymmetric stress state $S_{33} = S$, $S_{11} = S_{22} = S_T$, and for a linear viscous material one obtains

$$\dot{\delta} \approx 2.0[3.0S - 2.0S_T - \sigma_F]d/\mu \tag{B1}$$

$$\left.\begin{aligned} \dot{E} &\approx 0.6[4.6S - 3.6S_T - \sigma_F]/\mu. \\ \dot{E}_T &\approx -0.20[5.4S - 4.4S_T - \sigma_F]/\mu \end{aligned}\right\} \tag{B2}$$

Here, d is the diameter of the cavitated facet.

The effect of freely-sliding grain boundaries in an uncavitated uniaxially loaded specimen is estimated by setting $\dot{\delta} = 0$ and $S_T = 0$ in (B1). One then obtains $\sigma_F \approx 3.0S$, which determines the factor β for this second orientation as ≈ 3.0 compared to $\beta \approx 1.7$ when cavitated facets are hexagonal. Inserting $\sigma_F = 3.0S$ into the first of (B2) determines $\dot{E} \approx 2.9S/3\mu$ as compared to $\dot{E} \approx 1.6S/3\mu$ obtained for the first orientation of the Wigner–Seitz cell. Since $\dot{E} = S/3\mu$ when grain boundaries do not slide, the effect of such grain boundary sliding is to enhance $\dot{E}$ as seen before. Comparing strain rates for each of the orientations considered, grain boundary sliding is seen to introduce anisotropic response of the polycrystal even though the grain material is taken here to be isotropic.

The results (B1), (B2) may be interpreted for a nonlinear creeping grain material described by $\dot{\varepsilon}_{ij} = [\text{T-dependent factor}] \times \sigma^n$. An approximate effective viscosity $\mu(S, \sigma_F)$ of the grain, for use in (B1), (B2), is obtained in the manner described earlier. Here, $\mu(S, \sigma_F)$ has a weaker dependence on the value of σ_F than for the case of hexagonal cavitated facets. In fact, for this second orientation, the ratio of viscosities for a polycrystal with completely cavitated facets ($\sigma_F = 0$) to that for an uncavitated polycrystal ($\sigma_F = 3.0S$) is

$$\frac{\mu_{\text{complcav}}}{\mu_{\text{nocav}}} \approx \frac{1}{(1.7)^{n-1}}. \tag{B3}$$

We now develop for this second orientation expressions for $\dot{\delta}$ and $\dot{E}$, analogous to (10a,b) and (11a,b), that describe the limiting cases of well-separated and closely-spaced cavitated facets. In the former case, $\dot{\delta}$ is given by (1), using $\alpha = 1.8$ (corresponding to a polycrystal with freely-sliding grain boundaries and a creep exponent $n = 5$), $\beta = 3.0$ and $\dot{E}_{\text{nocav}}$ is given by the first of (B2), setting $\sigma_F = 3.0S$, $S_T = 0$ and $\mu = \mu(S, 3.0S)$. Also, $\dot{E} = \dot{E}_{\text{nocav}}$ for the well-separated geometry. In the latter case, $\dot{\delta}$ and $\dot{E}$ are given by (B1) and the first of (B2), respectively, setting $S_T = 0$ and evaluating $\mu = \mu(S, \sigma_F)$. Results are

$$\left.\begin{aligned} \dot{\delta} &\approx 0.58[3.0S - \sigma_F]d/\mu(S, 3.0S) \\ \dot{E} &\approx \dot{E}_{\text{nocav}} \approx 0.96S/\mu(S, 3.0S) \end{aligned}\right\} \text{(well-separated)} \tag{B4}$$

$$\left.\begin{aligned} \dot{\delta} &\approx 2.0[3.0S - \sigma_F]d/\mu(S, \sigma_F) \\ \dot{E} &\approx 0.60[4.6S - \sigma_F]/\mu(S, \sigma_F) \end{aligned}\right\} \text{(closely-spaced)}. \tag{B5}$$

Numerical results for nickel using this second orientation are presented in Fig. B2. Values of the void half-spacing b, facet diameter d and the material properties of nickel are unchanged from those used in Fig. 7 so that comparisons may be made. In essence, the functional forms of the t_r, E_r curves are similar for both orientations discussed, although the case of square cavitated facets produces lower times and strains to rupture, and the differences in t_r between well-separated and closely-spaced situations is somewhat less than when cavitated facets are hexagonal.